Journal of Innovative Optical Health Sciences
Vol. 10, No. 4 (2017) 1730004 (12 pages)

DOI: 10.1142/S179354581730004X

Photoacoustic molecular imaging with functional nanoparticles

Liming Liu and Huan Qin*
Ministry of Education Key Laboratory of Laser Life Science and Institute of Laser Life Science, College of Biophotonics
South China Normal University, Guangzhou 510631, P. R. China
**qinghuan@scnu.edu.cn*

Received 30 March 2017
Accepted 9 May 2017
Published 8 June 2017

Photoacoustic imaging (PAI) breaks through the optical diffusion limit by making use of the PA effect. By converting incident photons into ultrasonic waves, PAI combines high contrast of optical imaging and high spatial resolution in depth tissue of ultrasound imaging in a single imaging modality. This imaging modality has now shown potential for molecular imaging, which enables visualization of biological processes with systemically introduced functional nanoparticles. In the current review, the potentials of different optical nanoprobes as PAI contrast agents were elucidated and discussed.

Keywords: Photoacoustic imaging; optical nanoprobes; molecular imaging.

1. Introduction

Photoacoustic (PA) phenomenon was first discovered by Bell[1] in 1880. He observed a thin sheet of material exposed to a sunlight beam rapidly interrupted by a rotating slotted disk, emitted an audible sound signal and different materials produced different tones in his experience. However, the application of this technique had to wait almost a century until sensitive sensors and intense light sources for spectroscopy analysis development. In 1971, PA spectroscopy was reported to be sensitive enough to detect a concentration of 0.01 parts per million (ppm) of nitrogen oxide (NO_x) pollution in air samples.[2] In recent years, with the development of laser technology and biomedical nanotechnology, PA imaging (PAI) technology has become a hot research topic.[3–5]

The principle of PAI is illustrated in Fig. 1. When the pulse laser irradiation (thermoacoustic imaging, especially with the pulse of radio frequency laser irradiation) in biological tissue, tissue optical absorption domain will produce ultrasonic signal; we call this by ultrasonic signal as the excitation light produced by PA signal.[6–12] The PA signal generated by the biological tissue carries the information of optical absorption characteristics of the tissue, and the optical absorption distribution image can be reconstructed by detecting the PA signal.

*Corresponding author.

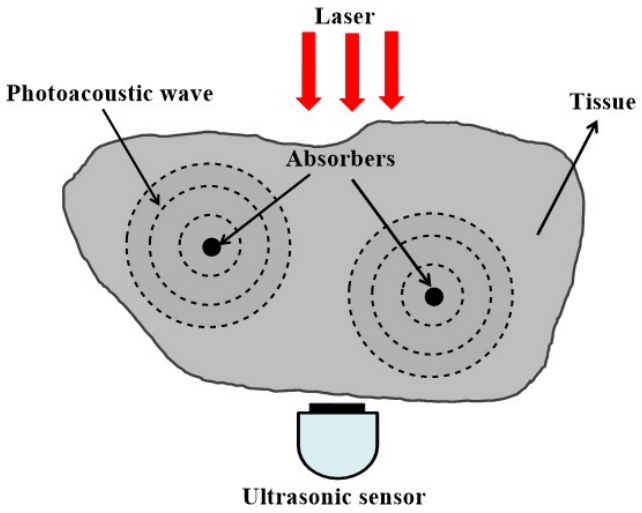

Fig. 1. The principle diagram of PAI.

PAI combines the advantages of characteristic selection and pure ultrasonic tissue imaging in deep tissue imaging in high pure optical transmission characteristics, can get image with high resolution and high contrast, from the principle of avoiding the influence of light scattering, breaking the high resolution optical imaging (OI) depth of "soft limit" (~1 mm), tissue imaging deep living can be realized within 50 mm.[13–30]

Nowadays, PA tomography (PAT) and PA microscopy (PAM) are the two important instrumental embodiments in PAI. PAT is widely recognized as a robust modality to evaluate the structure and function of biological tissues with high optical contrast and high acoustic resolution.[31–33] The combination of PAT with NP (NP) probes holds promises for detecting and imaging diseased tissues or monitoring their treatments with high sensitivity.[34] By ultrasonically overcoming the strong optical scattering, this imaging technology can reach penetration depth of centimeters while retaining high spatial resolution in biological tissue.[5] PAM refers to the imaging modality in which a PAI is captured by collecting signal pixel-by-pixel in an imaging grid. There are two types of PAM techniques depending on the resolution scale: acoustic-resolution PAM (AR-PAM) and optical-resolution PAM (OR-PAM). When a focussed ultrasound (US) detector is used, it is named AR-PAM because the imaging resolution is determined by the US propagation and detection. When a focussed laser beam is used, it is called OR-PAM because the resolution is dependent on the focussed laser beam size in the tissue.[35] In addition, some multimodality imaging methods are also widely used, such as PA/US imaging system; an integrated detector with sound-light coaxial/confocal design and flexible coupling mode is employed for the combined PA/US imaging strategy.[36–38] This method is able to simultaneously detect the absorption of chromophores such as hemoglobin and melanin and the differences in acoustic impedance.

There are both endogenous and exogenous PA contrast agents. Endogenous agents include hemoglobin,[39] melanin[40] and myoglobin[41] that manifest diseases depending on the chemical compositions of themselves. Nevertheless, many diseases and physiological processes usually reveal little or insufficient intrinsic PAI contrast. Therefore, it is highly essential and required to develop functional contrast agents for fully utilizing PAI potentials.

NPs play a more significant role in PAI. Various NPs can serve as PAI contrast agents such as gold nanorods (GNRs),[42–49] carbon[50,51] and polymer nanoprobe.[52,53] NPs can be made from a variety of responsive materials that produce signal only under the influence of a chemical cue. In this study, we discuss recent advances in NP contrast agents in PAI. We detail different materials and their properties as well as representative applications that demonstrate clear advantages in PAI. Finally, we discuss the challenges and broader impacts of PAI using functional NPs.

2. Application of Different Functional NPs in PAI

Generally, light energy is exponential decay with increasing tissue depth. Utilizing high-efficiency PA probes will be helpful for enhancing imaging contrast and therapy efficiency in deeper tissue. Functional NPs are important tools in PAI because they offer intense and stable signal and can be targeted to specific molecular processes. However, these probes have certain limitations and must be improved before they are widely applied in PA imaging. All in all, we divided the nanoprobes into two categories: inorganic and organic. Inorganic NPs include gold nanostructures, carbon nanotubes and graphene-based NP. These nanoprobes are successfully applied in PAI as contrast agents. This work also introduces the recent progress in organic NPs such as polymer NPs, which show improved

performance in structural and functional PA molecular imaging.

2.1. *Inorganic nanoprobes as PAI contrast agents*

Metal NPs have been employed for PA molecular tomography because of biocompatibility, easy for modifying the target, minimized toxicity and localized surface plasmon resonance (LSPR) peak as well as enhanced optical signals in near-infrared (NIR) spectral regions.[54–56] The optical absorption mechanism of different gold nanoconstructs such as GNRs, nanoshells, nanocages, nanostars, nanotripods and nanovesicles is based on LSPR.[5] The synthesis methods vary greatly for different kinds of particles. Gold forms strong gold-thiolate bonds that enable covalent surface modifications for optimizing biocompatibility (e.g., polyethylene glycol (PEG) functionalization),[57] stability (e.g., silica encapsulation)[58] and active targeting. By changing some crucial growth parameters, NPs in myriad shapes other than spheres can be obtained. More details about the synthesis procedures have been introduced in the literature.[54–60] Here, we take the GNRs as an example.

2.1.1. *Gold nanorods*

Among various gold nanostructures, GNR exhibits tunable, intense and narrow absorption peaks in the NIR region. These rod-shaped nanoprobes have attracted considerable attention as molecular probes for PAI of inflammatory response and tumor imaging. Gold-conjugated iron oxide NPs were used as dual modality agents for PA molecular tomography, compared with single GNRs, and it can produce much stronger shock waves by absorbing the optical energy and induced more efficient cell death at equal molar concentrations. In addition, gold forms strong gold-thiolate bonds that enable covalent surface modifications for optimizing biocompatibility such as the following: (1) gold NPs coated with gadolinium are used as contrasting agents for magnetic resonance imaging[72] and (2) folic-acid-conjugated GNRs are designed to specifically target folate receptor-expressing cancer cells and GNRs conjugated with FA as targeted absorbers were internalized into human epithelial carcinoma cells.[82]

As an alternative to molecular targeting ligands, peptides display high binding affinity and several advantages such as convenient synthesis and chemical modification, good tissue penetration, low immunogenicity, favorable pharmacokinetics and acceptable *in vivo* stability and integrity.[65,66] In this review, we enumerate iterative phage display selection to identify two novel high affinity binding oligopeptides selective and specific for UMR-106 cell. Then, the identified oligopeptides PT6 (PPTHPPP) and PT7 (PPSHTPT) were, respectively, conjugated to GNRs to develop specific nanoprobes for PAI of OS shown in Fig. 2(a).[53] Briefly, GNRs were synthesized according to a seed-mediated silver-assisted protocol.[54] Transmission electron microscope (TEM) images of oligopeptide-coated nanorods showed no change in morphology of nanorods (Figs. 2(b) and 2(c)). GNPs show the highest extinction coefficient in the NIR range and high PA conversion efficiency. PGNR-PT6 and -PT7 showed morphological and optical properties similar to unconjugated GNRs (shown in Fig. 2(d)). From Figs. 3(a) and 3(b), the results suggest that the oligopeptides might serve as a powerful vehicle for OS-specific therapeutic delivery, developing novel targeted oligopeptide–drug conjugates and refining OS treatment plans in clinical applications.

All in all, application of the GNRs reviewed here the aggregation concentration in blood vessels and tissues depend on their size, shape and synthetic route. Biocompatibility *in vivo* therefore needs to be more systematically addressed through a long period of time toxicity studies for individual nanostructures.

2.1.2. *Carbon NP*

Carbon forms different allotropic structures: carbon nanotubes, graphene-based nanomaterials and nanodiamonds. All three classes can be synthesized to possess an intrinsic absorption in the NIR range.[61] Especially interest is the wide variety of covalent[58–61] and noncovalent modifications with small molecules (dyes, drugs[59] or surfactants), polymers[59] and biomolecules,[60] which can be used for targeting, increased solubility and stability, improved signaling properties or increased specificity.

Over the past decade, single wall carbon nanotubes (SWNTs) with unique intrinsic property had been intensively explored for biological and biomedical applications. One intrinsic property of SWNTs is their ability to cross cellular membranes without eliciting cytotoxicity.[62] So as a unique quasi

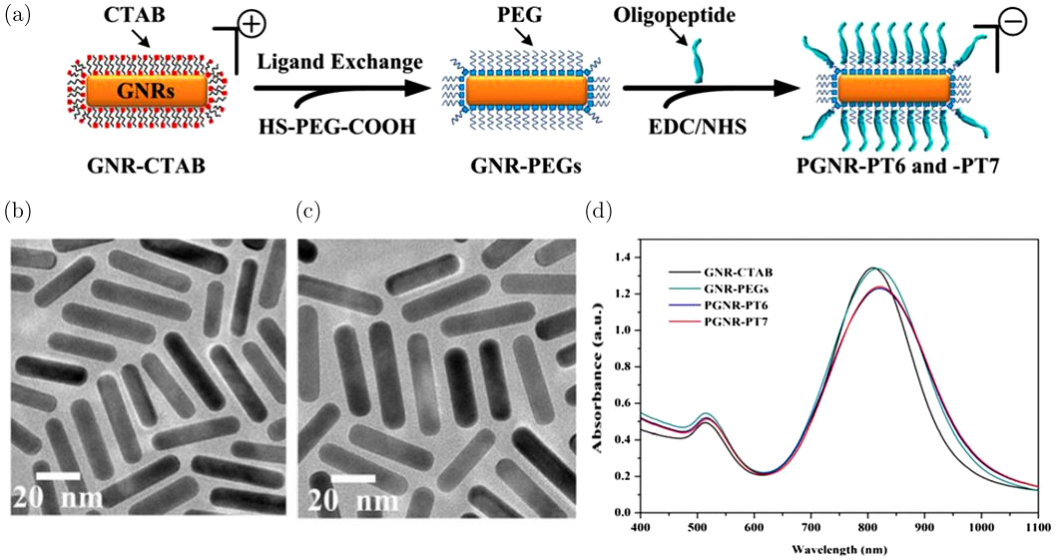

Fig. 2. (a) Synthesis of PEGylated GNRs with PT6 and PT7 oligopeptides. (b) and (c) TEM images of the PEGylated GNRs after modification with PT6 and PT7. (d) UV–Vis-NIR absorbance spectra of GNRs before (GNR-CTAB) and after PEGylation (GNR-PEGs) and oligopeptide conjugation (PGNR-PT6 and -PT7).

one-dimensional material, they have been explored as novel delivery vehicles for drugs,[63] proteins[64] and so on. Another intrinsic property of SWNTs is their strong optical absorbance in the NIR region,[65–68] which makes SWNTs appropriate to be used as agents for PAI.

The dye-enhanced contrast agent provided 300 times higher PA contrast in living tissues than sole

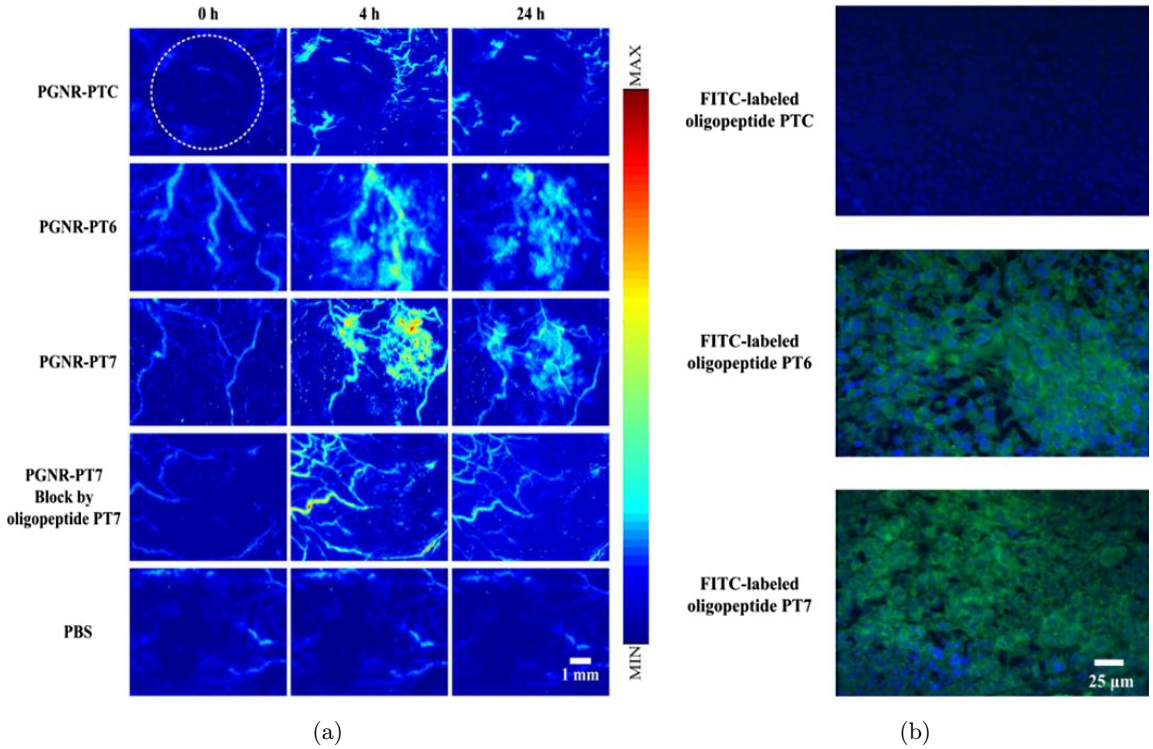

Fig. 3. (a) Sequential PA MIP frames of the tumor site before and after intravenous injection of PGNR-PTC, PGNR-PT6, PGNR-PT7, with pre-blocking and PBS at pre-administration (0 h), 4 h and 24 h after injection. (b) Representative fluorescence images of UMR-106 OS tissue sections stained with FITC-labeled PTC, PT6 or PT7 (100 nM).

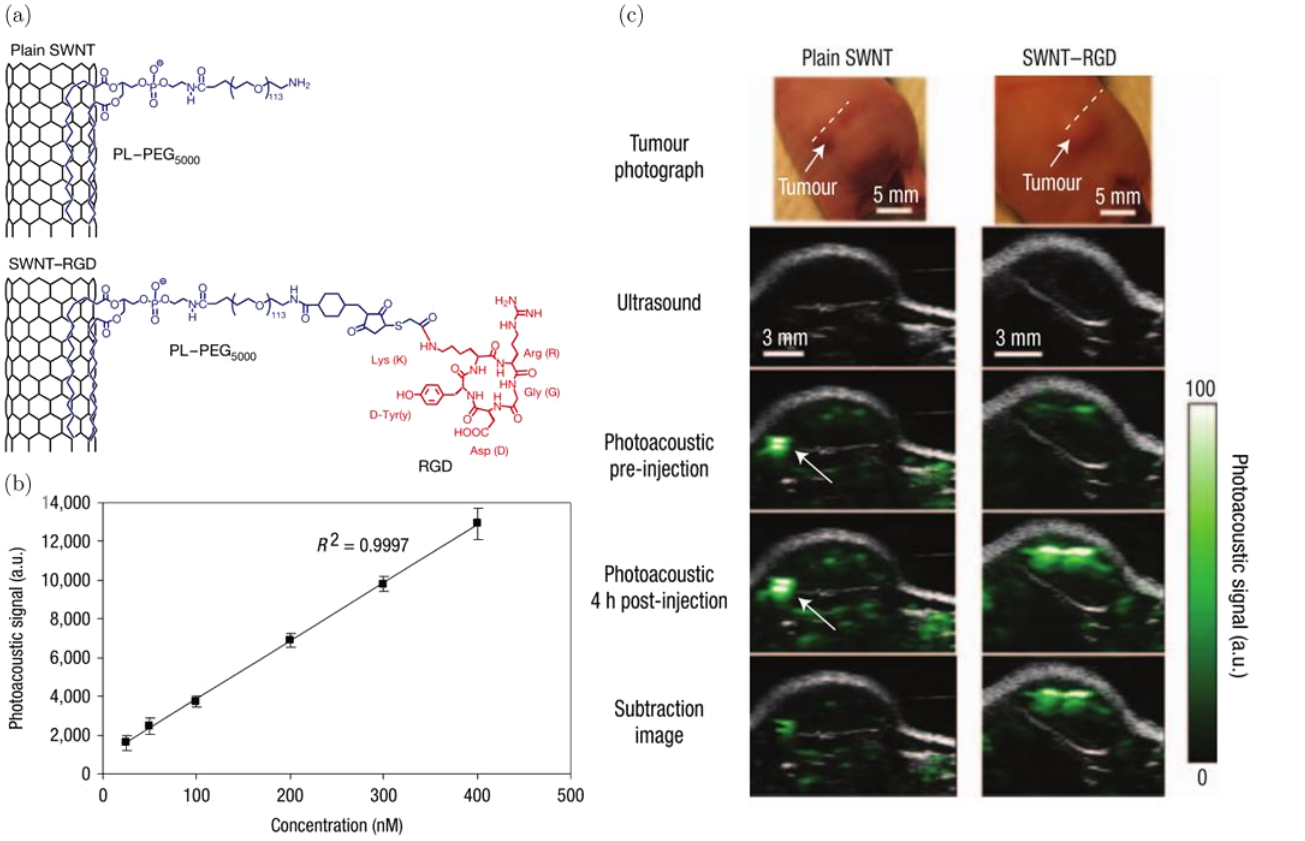

Fig. 4. (a) Schematic illustration of SWNTs conjugated with RGD peptides for targeted PAT of mouse tumor. (b) The PA signal produced by single-walled carbon nanotubes was observed to be linearly dependent on the concentration ($R^2 = 0.9997$). (c) B-scan US and PAIs of U87MG tumor acquired along a white dotted line aided by SWNTs. The ultrasound images (gray) show the skin and tumor boundaries, whereas PAT images (green) show optical absorption (SWNT–RGD) in the tumor. Differential images were obtained by subtraction of the pre-injection image from the 4 h post-injection image.

SWNT, leading to subnanomolar detection sensitivities. Approximately 20 times fewer U87MG cancer cells can be detectable by the combined agent than by sole SWNT. As carbon nanomaterials suffer from insolubility and efficient biocompatibility, a hyaluronic-acid-based biosurfactant was used to simultaneously disperse carbon NPs and target SWNT to CD44 receptor-positive tumor cells.[69–71] *In vivo* trimodality PAT/fluorescence/PET imaging of coated SWCNTs showed high tumor targeting ability while providing long-term monitoring of enzyme events. An SWNT conjugated with cyclic Arg-Gly-Asp (RGD) peptides can be used as a contrast agent for PAI of tumours.[41] These SWNT–RGD conjugates bind with high affinity to $\alpha_\nu\beta_3$ integrin, which is overexpressed in tumor neovasculature, and to other integrins expressed by tumours but with lower affinity.[18,19] The synthesis scheme of SWNT (plain SWNT) and SWNT–RGD are shown in Fig. 4(a). From Fig. 4(b), we also validated that the PA signal produced by SWNTs is in linear relationship with their concentration with $R^2 = 0.9997$. Three-dimensional US and PAIs of the mice-bearing U87MG tumors were shown in Fig. 4(c). In addition, the surroundings were acquired before and up to 4 h after injection. The figure shows that the PA signal in the tumor mice injected with SWNT–RGD increase obviously then control mice injected with plain SWNTs. This article illustrated that SWNTs were able to efficiently bind to molecular targets, and their high PA signal allows for high-resolution 3D PAIs with substantial depth of penetration and could present a unique set of features.[72]

2.1.3. *Graphene oxide in PAI*

Graphene is a 2D free-standing honeycomb lattice made of a single atomic plane of graphite. Compared with carbon nanotubes, graphene is a new carbon material structure with a large number of

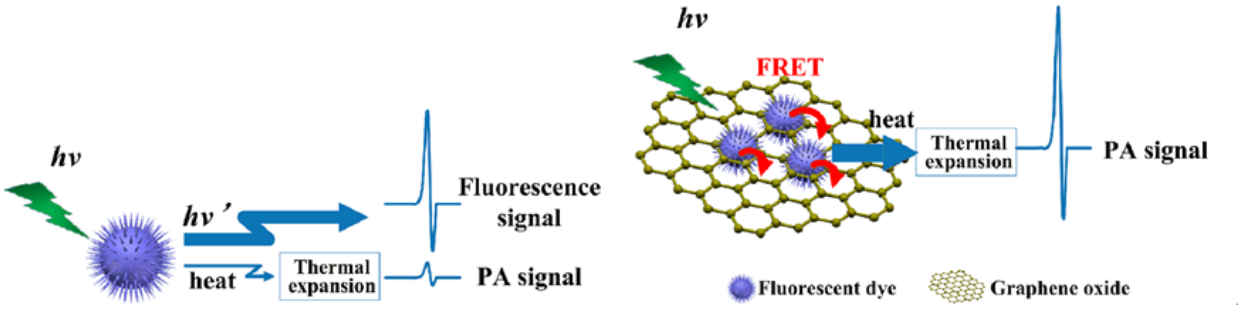

(a) (b)

Fig. 5. (a) Fluorescent dyes with strong absorption, strong fluorescence and weak thermoelastic wave characteristics and (b) π–π stacking of dyes in close proximity to GO. GO quenches the dye fluorescence via FRET between dye molecules and GO. Using the pulse laser irradiation, the vast majority of absorbed light energy is converted to acoustic waves.

surface oxygen groups, with good solubility, affinity and polymer. Using strong oxidizing agents, oxygenated functionalities in the graphene structure can produce graphene oxide (GO), which is hydrophilic and more biocompatible.[73–78] Here we enumerate a probe with the highest availability of optical-thermo conversion by using GO and dyes via π–π stacking interactions. The attached dye molecules on GO can selectively absorb light energy due to their narrow absorption spectral profile. GO efficiently quenches the dye fluorescence via fluorescence resonance energy transfer (FRET) between the dyes and GO, enabling the absorbed light energy to be converted into thermal energy. With a pulse laser, the absorbed light energy of GO dyes would efficiently convert to acoustic waves via the PA effect (Fig. 5). This study shows that GO quenches the attached dye fluorescence via FRET, resulting in higher PA signal than the sum of the separate signals generated in the dye and the GO (Fig. 6).

These kinds of carbon nanotubes have intrinsic absorption in the NIR range. Future work of fluorescent molecules in PAT is needed to further increase the conversion efficiency of laser energy to acoustic emission. In conclusion, carbon as a good biocompatibility of the nanoprobe can be further developed and utilized.

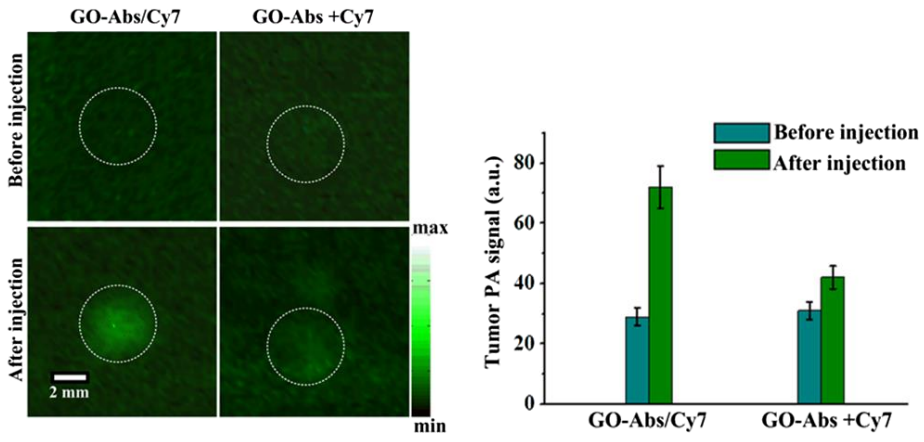

(a) (b)

Fig. 6. Comparison of PAI contrast of tumors after being injected with GO–Abs/Cy7, GO–Abs and Cy7. (a) The first group of U87-bearing Balb/c nude mice ($n = 3$) was injected through the tail vein (IV) with GO–Abs/Cy7 (the first row). In the second group ($n = 3$), separate GO–Abs and Cy7 solutions were injected simultaneously into the same mice (the second row). The PAI in the first line represents the mouse group before injection and the second line represents the mouse 6 h after being injected with GO-Abs/Cy7 or GO-Abs plus Cy7. The white dotted lines on the images illustrate the approximate tumor edges. (b) Quantification of the signals in the tumor shows higher in the PA image after injecting GO-Abs/Cy7 compared to before injection and in the other group (the injection of GO-Abs and Cy7 in the same mouse). The error bars represent standard error ($n = 3$ mice).

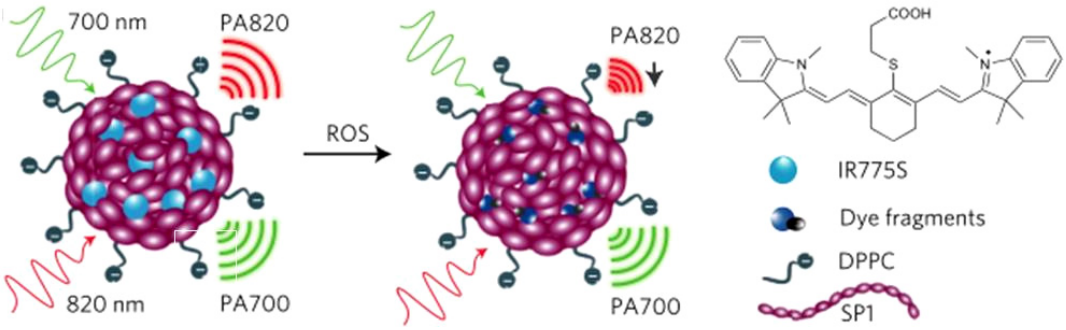

Fig. 7. *In vitro* characterization of RSPN for ROS sensing. Proposed ROS sensing mechanism.

2.2. *Organic nanoprobes as PAI contrast agents*

2.2.1. *Polymer NPs*

PAI holds great promise for the visualization of physiology and pathology at the molecular level with deep tissue penetration and fine spatial resolution. Here, we refer NIR light-absorbing semiconducting polymer NPs: semiconducting polymer nanoparticles (SPNs) as a new class of contrast agents for PA molecular imaging.[62]

Recently, SPNs have been transformed as efficient PA and fluorescent imaging nanomaterials. Specifically, two semiconducting polymer derivatives, poly(cyclopentadithio-phene-alt-benzothiadiazole) (SP1) and poly(acenaphthothieno-pyrazine-alt-benzodithiophene) (SP2), with molecular structure were used to prepare functional SPNs.[68] The imaging of reaction oxygen species (ROS) is critical to understanding the etiology of disease and to optimize therapeutic interventions against potentially life-threatening conditions. SPN1 itself has high stability toward ROS, so we coupled it to a cyanine dye derivative (IR775S) that is sensitive to ROS-mediated oxidation to design a ratiometric photoacoustic probe (RSPN) for ROS imaging (Fig. 7). One-pot nanoprecipitation process produced water-soluble functional SPNs at a small diameter (45 nm) and good size stability for ratiometric PA detection.

RSPN was applied for the *in vivo* PA molecular tomography of ROS in a murine model of acute edema. The PA signal was simultaneously monitored at 700 and 820 nm, as illustrated by pseudo green and red colors, respectively. The PA amplitude at 700 nm for both saline and zymosan-treated mice remained nearly unchanged over time (Fig. 8(a)). The progressive enlargement in the

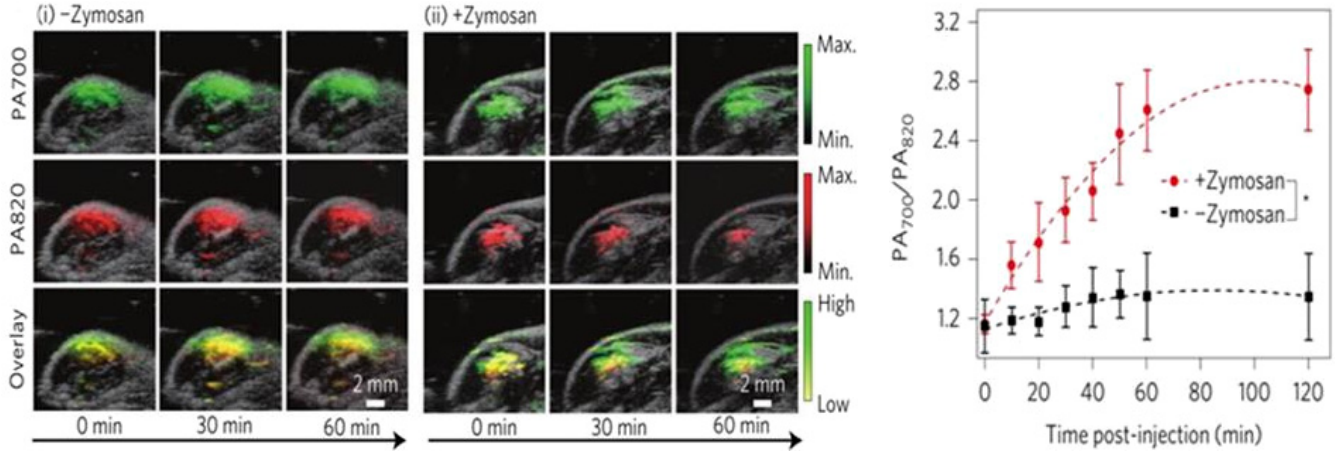

(a) (b)

Fig. 8. *In vivo* PAT of ROS generation from a mouse model of acute edema using RSPN.[56] (a) PA/US overlaid images of saline-treated (i) and zymosan-treated (ii) regions in the thigh of living mice ($n = 3$). (b) Ratio of PA amplitude at 700 nm to that at 820 nm (PA_{700}/PA_{820}) as a function of time post-injection of RSPN.

signaling area was attributed to tissue diffusion of NPs over time. In contrast, both the PA amplitude and the area of signal production at 820 nm for zymosan-treated mice significantly decreased over time (Fig. 8(a)). The superposition analysis delineated a progressive pseudocolor variation from yellow to green for zymosan-treated mice but not for control mice (Fig. 8(a)), indicating the *in situ* generation of inflammatory ROS during edema. Quantitative analysis revealed that PA 700/PA 820 gradually increased to 2.7+0.31 at 120 min post-injection for zymosan-treated mice, which was significantly elevated relative to control mice (1.4+0.22) (Fig. 8(b)). Thus, RSPN effectively detected *in vivo* ROS production using a dual-peak ratiometric PA contrast mechanism, demonstrating the potential of SPNs for activate PAI of the progression of pathological processes in real time.

This study demonstrated the feasibility of SPN for activatable PA detection of pathological ROS change by a dual-peak ratiometric contrast mechanism. However, the biosafety of the polymer materials should be mass survey. Another information we can find in this study is that ROS characteristics of some chronic diseases may not be sensitive enough to be distinguished by this approach.

3. Different PAI Nano Probes for Different *In Vivo* Applications

Different functions and properties of nanoprobes have different applications *in vivo* PAI. Pu *et al.*[34] have developed an activated NIR PA probe[51] with properties such as the narrow PA spectral profile, good photostability, for *in vivo* imaging of ROS, a hallmark of many pathological processes such as cancer, stroke and bacterial infections. SPN-based PA probes effectively detect ROS and exhibit great enhancements in ratiometric PA signals (PA 700/PA 820) of 25, 7.3 and 2.7 times in solution, in cells and in living mice (Fig. 8). Liu *et al.* have reported a novel activatable PAI nanoprobe[79] for *in vivo* detection of cancer-related matrix metalloproteinases (MMPs). A black hole quencher 3 (BHQ3) which absorbs red light is conjugated to NIR-absorbing copper sulfide (CuS) NPs via an MMP-cleavable peptide linker. The obtained CuS-peptide-BHQ3 (CPQ) nanoprobe exhibits two distinctive absorption peaks at 630 and 930 nm. Inside the tumor microenvironment where MMPs are present, the MMP-sensitive peptide would be cleaved, releasing BHQ3 from the CuS nanoparticles; the former as a small molecule is then rapidly cleared out from the tumor and the latter of which as large nanoparticles would retain inside the tumor for a much longer time. Such a simple and straightforward strategy allowed us to use PAI for *in vivo* detection of a specific enzyme activity. Compared with traditional OI used in MMP detection, PAI would exhibit dramatically enhanced penetration of tissues and is expected to offer markedly improved *in vivo* spatial resolution during imaging owing to its unique mechanism. Altogether, the choice of different nanoprobes for PAI depends on nanoprobes properties and biological interactions.

4. Discussion and Conclusion

Molecular imaging techniques existing in time and spatial resolution, depth of penetration, ductility, energy availability and probe detection limits have their advantages and disadvantages, and a variety of imaging technologies combined will provide more comprehensive information. The design of multifunctional imaging probe now is a concrete measure of future development of molecular imaging well not only in the condition of various kinds of imaging technology but also has a therapeutic effect. However, the particle size, material composition, shape, surface chemical properties, the biological activity of the ligand, the imaging effect of the probe, the biological safety of the probe and other factors affect the clinical application of step.

In this review, we have listed some recent contrast agent advancements in design, biochemistry and theranostic applications for PAI. Indeed, the versatile optical probes are now increasingly active in numerous aspects: enhanced sensitivity and specificity, functional biosensing, activatable drug release/response and imaging of tumor microenvironments. However, there is no single best agent for all applications and selection of the most ideal agent can be ambiguous due to the great variety of NPs.

In summary, it is expected that further advancement of this fast-growing topic will continue to accelerate both basic life sciences and bedside clinic care. In addition, we hope that PA molecular imaging with functional nanoparticles will be widely used in potential clinical applications.

Acknowledgments

This research is supported by the National Natural Science Foundation of China (11604105; 61627827; 81630046; 61331001; 91539127; 61361160414), The National High Technology Research and Development Program of China (2015AA020901) and The Science and Technology Planning Project of Guangdong Province, China (2015B020233016 and 2014B020215003).

References

1. A. G. Bell, "On the production and reproduction of sound by light," *Am. J. Sci.* **118**, 305–324 (1880).
2. L. B. Kreuzer, C. K. N. Patel, "Nitric oxide air pollution: Detection by optoacoustic spectroscopy," *Science* **173**, 45–47 (1971).
3. C. Kim, C. Favazza, L. V. Wang, "*In vivo* photoacoustic tomography of chemicals: High-resolution functional and molecular optical imaging at new depths," *Chem. Rev.* **110**, 2756–2782 (2010).
4. L. V. Wang, H. Song, "Photoacoustic tomography: *In vivo* imaging from organelles to organs," *Science* **335**, 1458–1462 (2012).
5. L. Nie, X. Chen, "Structural and functional photoacoustic molecular tomography aided by emerging contrast agents," *Chem. Soc. Rev.* **43**, 7132–7170 (2014).
6. L. V. Wang, J. Yao, "A practical guide to photoacoustic tomography in the life sciences," *Nat. Meth.* **13**, 627–638 (2016).
7. Y. Shi L. Xiang, Y. Yuan, D. Xing, Z. Ou, F. Zhou, "Thermally confined shell coating amplifies the photoacoustic conversion efficiency of nanoprobes," *Nano Res.* **9**, 3644–3655 (2016).
8. A. Taruttis, G. M. van Dam, V. Ntziachristos, "Mesoscopic and macroscopic optoacoustic imaging of cancer," *Cancer Res.* **75**, 1548–1559 (2015).
9. S. Yang, D. Xing, Q. Zhou, L. Xiang, Y. Lao, "Functional imaging of cerebrovascular activities in small animals using high-resolution photoacoustic tomography," *Med. Phys.* **34**, 3294–3301 (2007).
10. P. Beard, "Biomedical photoacoustic imaging," *Interf. Focus* **1**, 602–631 (2011).
11. A. De La Zerda, C. Zavaleta, S. Keren, S. Vaithilingam, S. Bodapati, Z. Liu, Z. Cheng, "Carbon nanotubes as photoacoustic molecular imaging agents in living mice," *Nat. Nanotechnol.* **3**, 557–562 (2008).
12. Y. Lao, D. Xing, S. Yang, L Xiang, "Noninvasive photoacoustic imaging of the developing vasculature during early tumor growth," *Phys. Med. Biol.* **53**, 4203 (2008).
13. M. Xu, L. V. Wang, "Photoacoustic imaging in biomedicine," *Rev. Sci. Instrum.* **77**, 041101 (2006).
14. X. Michalet, F. F. Pinaud, L. A. Bentolila, J. M. Tsay, S. J. J. L. Doose, J. J. Li, S. Weiss, "Quantum dots for live cells, *in vivo* imaging, and diagnostics," *Science* **307**(5709), 538–544 (2005).
15. P.-C. Li, C.-R. Chris Wang, D.-B. Shieh, C.-W. Wei, C.-K. Liao, C. Poe, S. Jhan, A.-A. Ding, Y.-N. Wu, "*In vivo* photoacoustic molecular imaging with simultaneous multiple selective targeting using antibody-conjugated gold nanorods," *Opt. Express.* **16**, 18605–18615 (2008).
16. L. Xiang, Y. Yuan, D. Xing, Z. Ou, S. Yang, F. Zhou, "Photoacoustic molecular imaging with antibody-functionalized single-walled carbon nanotubes for early diagnosis of tumor," *J. Biomed. Opt.* **14**, 021008–021008-7 (2009).
17. C. Li, L. V. Wang. "Photoacoustic tomography and sensing in biomedicine," *Phys. Med. Biol.* **54**, R59 (2009).
18. G. Huang, S. Yang, Y. Yuan, D. Xing, "Combining X-ray and photoacoustics for *in vivo* tumor imaging with gold nanorods," *Appl. Phys. Lett.* **99**, 123701 (2011).
19. S. Mallidi, T. Larson, J. Tam, P. P. Joshi, A. Karpiouk, K. Sokolov, S. Emelianov, "Multiwavelength photoacoustic imaging and plasmon resonance coupling of gold nanoparticles for selective detection of cancer," *Nano Lett.* **9**, 2825–2831 (2009).
20. I. Pastoriza-Santos, J. Pérez-Juste, L. M. Liz-Marzán, "Silica-coating and hydrophobation of CTAB-stabilized gold nanorods," *Chem. Mater.* **18**, 2465–2467 (2006).
21. J. V. Jokerst, A. J. Cole, D. Van de Sompel, S. S. Gambhir, "Gold nanorods for ovarian cancer detection with photoacoustic imaging and resection guidance via Raman imaging in living mice," *ACS Nano* **6**, 10366–10377 (2012).
22. H. Qin, T. Zhou, S. Yang, D. Xing, "Fluorescence quenching nanoprobes dedicated to *in vivo* photoacoustic imaging and high-efficient tumor therapy in deep-seated tissue," *Small* **11**, 2675–2686 (2015).
23. Y. Zhao, S. Yang, C. Chen, D. Xing, "Simultaneous optical absorption and viscoelasticity imaging based on photoacoustic lock-in measurement," *Opt. Lett.* **39**, 2565–2568 (2014).
24. J. Zhong, S. Yang, X. Zheng, T. Zhou, D. Xing, "*In vivo* photoacoustic therapy with cancer-targeted indocyanine green-containing nanoparticles," *Nanomedicine* **8**, 903–919 (2013).
25. Z. Chen, S. Yang, D. Xing, "*In vivo* detection of hemoglobin oxygen saturation and carboxyhemoglobin saturation with multiwavelength photoacoustic microscopy," *Opt. Lett.* **37**, 3414–3416 (2012).

26. G. Gao, S. Yang, D. Xing, "Viscoelasticity imaging of biological tissues with phase-resolved photoacoustic measurement," *Opt. Lett.* **36**, 3341–3343 (2011).
27. F. Ye, S. Yang, D. Xing, "Three-dimensional photoacoustic imaging system in line confocal mode for breast cancer detection," *Appl. Phys. Lett.* **97**, 213702 (2010).
28. H. Wang, D. Xing, L. Xiang, "Photoacoustic imaging using an ultrasonic Fresnel zone plate transducer," *J. Phys. D Appl. Phys.* **41**, 095111 (2008).
29. Y. Yuan, S. Yang, D. Xing, "Optical-resolution photoacoustic microscopy based on two-dimensional scanning galvanometer," *Appl. Phys. Lett.* **100**(2), 023702 (2012).
30. B. Li, H. Qin, S. Yang, D. Xing, "*In vivo* fast variable focus photoacoustic microscopy using an electrically tunable lens," *Opt. Express.* **22**, 20130–20137 (2014).
31. Y. Wang, X. Xie, X. Wang, G. Ku, K. L. Gill, D. P. O'Neal, G. Stoica, L. V. Wang, "Photoacoustic tomography of a nanoshell contrast agent in the *in vivo* rat brain," *Nano Lett.* **9**, 1689–1692 (2004).
32. C. Kim, C. Favazza, L. V. Wang, "*In vivo* photoacoustic tomography of chemicals: High-resolution functional and molecular optical imaging at new depths," *Chem. Rev.* **110**, 2756–2782 (2010).
33. H. Chen, Z. Yuan, C. Wu, "Nanoparticle probes for structural and functional photoacoustic molecular tomography," *BioMed Res. Int.* **2015**, (2015).
34. K. Pu, A. J. Shuhendler, J. V. Jokerst, J. Mei, S. S. Gambhir, Z. Bao, J. Rao, "Semiconducting polymer nanoparticles as photoacoustic molecular imaging probes in living mice," *Nat. Nanotechnol.* **9**, 233–239 (2014).
35. Y. Lyu, Y. Fang, Q. Miao, X. Zhen, D. Ding, K. Pu, "Intraparticle molecular orbital engineering of semiconducting polymer nanoparticles as amplified theranostics for *in vivo* photoacoustic imaging and photothermal therapy," *ACS Nano* **10**, 4472–4481 (2016).
36. Y. Wang, D. Xu, S. Yang, D. Xing, "Toward *in vivo* biopsy of melanoma based on photoacoustic and ultrasound dual imaging with an integrated detector," *Biomed. Opt. Express* **7**, 279–286 (2016).
37. Y. Wang, S. Hu, K. Maslov, Y. Zhang, Y. Xia, L. V. Wang, "*In vivo* integrated photoacoustic and confocal microscopy of hemoglobin oxygen saturation and oxygen partial pressure," *Opt. Lett.* **36**, 1029–1031 (2011).
38. J. A. Viator, L. O. Svaasand, G. Aguilar, B. Choi, J. Stuart Nelsonw, "A comparative study of photoacoustic and reflectance methods for determination of epidermal melanin content," *J. Invest. Dermatol.* **122**, 1432–1439 (2004).
39. M. Holotta, H. Grossauer, C. Kremser, P. Torbica, J. Volkl, G. Degenhart, R. Esterhammer, R. Nuster, G. Paltauf, W. Jaschke, "Photoacoustic tomography of *ex vivo* mouse hearts with myocardial infarction," *J. Biomed. Opt.* **16**, 036007–036007-5 (2011).
40. J. Wang, B. Dong, B. Chen, Z. Jiang, H. Song, "Selective photothermal therapy for breast cancer with targeting peptide modified gold nanorods," *Dalton Trans.* **41**, 11134–11144 (2012).
41. D. L. Chamberland, A. Agarwal, N. Kotov, J. B. Fowlkes, P. L. Carson, X. Wang, "Photoacoustic tomography of joints aided by an Etanercept-conjugated gold nanoparticle contrast agent — an *ex vivo* preliminary rat study," *Nanotechnology* **19**, 095101 (2008).
42. Q. Zhang, N. Wang, P. Sharma, B. M. Moudgil, C. Wu, J. McNeill, H. Jiang, S. R. Grobmyer, "Gold nanoparticles as a contrast agent for *in vivo* tumor imaging with photoacoustic tomography," *Nanotechnology* **20**, 395102 (2009).
43. S. Yang, F. Ye, D. Xing, "Intracellular label-free gold nanorods imaging with photoacoustic microscopy," *Opt. Express.* **20**, 10370–10375 (2012).
44. H. Qin, T. Zhou, S. Yang, Q. Chen, D. Xing, "Gadolinium (III)-gold nanorods for MRI and photoacoustic imaging dual-modality detection of macrophages in atherosclerotic inflammation," *Nanomedicine* **8**, 1611–1624 (2013).
45. K. Kim, S.-W. Huang, S. Ashkenazi, M. O'Donnell, A. Agarwal, N. A. Kotov, M. F. Denny, M. J. Kaplan, "Photoacoustic imaging of early inflammatory response using gold nanorods," *Appl. Phys. Lett.* **90**, 223901 (2007).
46. M. Eghtedari, A. Oraevsky, J. A. Copland, N. A. Kotov, A. Conjusteau, M. Motamedi, "High sensitivity of *in vivo* detection of gold nanorods using a laser optoacoustic imaging system," *Nano Lett.* **7**, 1914–1918 (2007).
47. A. De La Zerda, C. Zavaleta, S. Keren, S. Vaithilingam, S. Bodapati, Z. Liu, J. Levi, B. R. Smith, T.-J. Ma, O. Oralkan, Z. Cheng, X. Chen, H. Dai, B. T. Khuri-Yakub, S. S. Gambhir, "Carbon nanotubes as photoacoustic molecular imaging agents in living mice," *Nat. Nanotechnol.* **3**, 557–562 (2008).
48. A. De La Zerda, Z. Liu, S. Bodapati, R. Teed, S. Vaithilingam, B. T. Khuri-Yakub, X. Chen, H. Dai, S. S. Gambhir, "Ultrahigh sensitivity carbon nanotube agents for photoacoustic molecular imaging in living mice," *Nano Lett.* **10**, 2168–2172 (2010).
49. K. Li, B. Liu, "Polymer-encapsulated organic nanoparticles for fluorescence and photoacoustic imaging," *Chem. Soc. Rev.* **43**, 6570–6597 (2014).
50. Z. Ma, H. Qin, H. Chena, H. Yanga, J. Xua, S. Yang, J. Hu, D. Xing, "Phage display-derived

oligopeptide-functionalized probes for *in vivo* specific photoacoustic imaging of osteosarcoma," *Nanomed. Nanotechnol. Biol. Med.* **13**, 111–121 (2017).
51. X. Ye, L. Jin, H. Caglayan, J. Chen, G. Xing, C. Zheng, V. Doan-Nguyen, Y. Kang, N. Engheta, C. R. Kagan, C. B. Murray, "Improved size-tunable synthesis of monodisperse gold nanorods through the use of aromatic additives," *ACS Nano* **6**, 2804–2817 (2012).
52. J. Choi, J. Yang, D. Bang, J. Park, J. S. Suh, Y. M. Huh, S. Haam, "Targetable gold nanorods for epithelial cancer therapy guided by near-IR absorption imaging," *Small* **8**, 746–753 (2012).
53. M. Grzelczak, J. Pérez-Juste, P. Mulvaney, L. M. Liz-Marzán, "Shape control in gold nanoparticle synthesis," *Chem. Soc. Rev.* **37**, 1783–1791 (2008).
54. A. E. Porter, M. Gass, K. Muller, J. N. Skepper, P. A. Midgley, M. Welland, "Direct imaging of single-walled carbon nanotubes in cells," *Nat. Nanotechnol.* **2**, 713–717 (2007).
55. Z. Liu, K. Chen, C. Davis, S. Sherlock, Q. Cao, X. Chen, H. Dai, "Drug delivery with carbon nanotubes for *in vivo* cancer treatment," *Cancer Res.* **68**, 6652–6660 (2008).
56. N. W. Shi Kam, T. C. Jessop, P. A. Wender, H. Dai, "Nanotube molecular transporters: Internalization of carbon nanotube-protein conjugates into mammalian cells," *J. Am. Chem. Soc.* **126**, 6850–6851 (2004).
57. M. J. O'Connell, S. M. Bachilo, C. B. Huffman, V. C. Moore, M. S. Strano, E. H. Haroz, K. L. Rialon, P. J. Boul, W. H. Noon, C. Kittrell, J. Ma, R. H. Hauge, R. B. Weisman, R. B. Smalley, "Band gap fluorescence from individual single-walled carbon nanotubes," *Science* **297**, 593–596 (2002).
58. N. W. Shi Kam, M. O'Connell, J. A. Wisdom, H. Dai, "Carbon nanotubes as multifunctional biological transporters and near-infrared agents for selective cancer cell destruction," *Proc. Natl Acad. Sci. USA* **102**, 11600–11605 (2005).
59. L. Wen, W. Ding, S. Yang, D. Xing, "Microwave pumped high-efficient thermoacoustic tumor therapy with single wall carbon nanotubes," *Biomaterials* **75**, 163–173 (2016).
60. M.-C. Daniel, D. Astruc, "Gold nanoparticles: Assembly, supramolecular chemistry, quantum-size-related properties, and applications toward biology, catalysis, and nanotechnology," *Chem. Rev.* **104**, 293–346 (2004).
61. Y.-S. Chen, W. Frey, S. Kim, K. Homan, P. Kruizinga, K. Sokolov, S. Emelianov, "Enhanced thermal stability of silica-coated gold nanorods for photoacoustic imaging and image-guided therapy," *Opt. Express* **18**, 8867–8878 (2010).
62. S. L. Deutscher, "Phage display in molecular imaging and diagnosis of cancer," *Chem. Rev.* **110**, 3196–3211 (2010).
63. S. Lee, J. Xie, X. Chen, "Peptide-based probes for targeted molecular imaging," *Biochemistry* **49**, 1364–1376 (2010).
64. K. Chen, P. S. Conti, "Target-specific delivery of peptide-based probes for PET imaging," *Adv. Drug Deliv. Rev.* **62**, 1005–1022 (2010).
65. J. Enbäck, P. Laakkonen, "Tumour-homing peptides: Tools for targeting, imaging and destruction," 780–783 (2007).
66. J. Weber, P. C. Beard, S. E. Bohndiek, "Contrast agents for molecular photoacoustic imaging," *Nat. Meth.* **13**, 639–650 (2016).
67. M. Zhang, M. Yudasaka, K. Ajima, J. Miyawaki, S. Iijima, "Light-assisted oxidation of single-wall carbon nanohorns for abundant creation of oxygenated groups that enable chemical modifications with proteins to enhance biocompatibility," *ACS Nano* **1**, 265–272 (2007).
68. A. Krueger, L. Daniel, "Functionality is key: Recent progress in the surface modification of nanodiamond," *Adv. Funct. Mater.* **22**, 890–906 (2012).
69. H. He, C. Gao, "General approach to individually dispersed, highly soluble, and conductive graphene nanosheets functionalized by nitrene chemistry," *Chem. Mater.* **22**, 5054–5064 (2010).
70. J. L. Bahr, J. Yang, D. V. Kosynkin, M. J. Bronikowski, R. E. Smalley, J. M. Tour, "Functionalization of carbon nanotubes by electrochemical reduction of aryl diazonium salts: A bucky paper electrode," *J. Am. Chem. Soc.* **123**, 6536–6542 (2001).
71. A. de la Zerda, S. Bodapati, R. Teed, S. Y. May, S. M. Tabakman, Z. Liu, B. T. Khuri-Yakub, X. Chen, H. Dai, S. S. Gambhir, "Family of enhanced photoacoustic imaging agents for high-sensitivity and multiplexing studies in living mice," *ACS Nano* **6**, 4694–4701 (2012).
72. Z. Liu, J. T. Robinson, X. Sun, H. Dai, "PEGylated nanographene oxide for delivery of water-insoluble cancer drugs," *J. Am. Chem. Soc.* **130**, 10876–10877 (2008).
73. M. J. O'Connell, S. M. Bachilo, C. B. Huffman, V. C. Moore, M. S. Strano, E. H. Haroz, K. L. Rialon, P. J. Boul, W. H. Noon, C. Kittrell, J. Ma, R. H. Hauge, R. Bruce Weisman, R. E. Smalley, "Band gap fluorescence from individual single-walled carbon nanotubes," *Science* **297**, 593–596 (2002).
74. Y. Shao, J. Wang, H. Wu, J. Liu, I. A. Aksay, Y. Lin, "Graphene based electrochemical sensors and biosensors: A review," *Electroanalysis* **22**, 1027–1036 (2010).

75. M. Swierczewska, K. Young Choi, E. L. Mertz, X. Huang, F. Zhang, L. Zhu, H. Yeol Yoon, J. Hyung Park, A. Bhirde, S. Lee, X. Chen, "A facile, one-step nanocarbon functionalization for biomedical applications," *Nano Lett.* **12**, 3613–3620 (2012).
76. P. Padmanabhan, A. Kumar, S. Kumar, R. K. Chaudhary, B. Gulyás, "Nanoparticles in practice for molecular-imaging applications: An overview," *Acta Biomaterialia* **41**, 1–16 (2016).
77. W. He, K. Ai, C. Jiang, K. Ai, C. Jiang, Y. Li, X. Song, L. Lu, "Plasmonic titanium nitride nanoparticles for *in vivo* photoacoustic tomography imaging and photothermal cancer therapy," *Biomaterials* (2017).
78. R. Alwi, S. Telenkov, A. Mandelis, A. Mandelis, T. Leshuk, F. Gu, S. Oladepo, K. Michaelian, "Silica-coated super paramagnetic iron oxide nanoparticles (SPION) as biocompatible contrast agent in biomedical photoacoustics," *Biomed. Opt. Express* **10**, 2500–2509 (2012).
79. K. Yang, L. Zhu, L. Nie, X. Sun, L. Cheng, C. Wu, G. Niu, X. Chen, Z. Liu, "Visualization of protease activity *in vivo* using an activatable photo-acoustic imaging probe based on CuS nanoparticles," *Theranostics* **4**, 134–141 (2014).